INTERNATIONAL JOURNAL FOR NUMERICAL METHODS IN ENGINEERING
Int. J. Numer. Meth. Engng 0000; **00**:1–20
Published online in Wiley InterScience (www.interscience.wiley.com). DOI: 10.1002/nme

Exploration of Efficient Reduced-Order Modeling and A Posteriori Error Estimation

J. H. Chaudhry[1], D. Estep[2*], and M. Gunzburger[3]

[1] *Department of Mathematics and Statistics, The University of New Mexico, Albuquerque, 87131.*
[2] *Department of Statistics, Colorado State University, Fort Collins, CO, 80523.*
[3] *Department of Scientific Computing, Florida State University, Tallahassee, FL, 32306.*
J. Chaudhry's work is supported in part by the Department of Energy (DE-SC0009279, DE-SC0009324). D. Estep's work is supported in part by the Department of Energy (DE-SC0009279). M. Gunzburger's work is partially supported by the Department of Energy (DE-SC0009324).

SUMMARY

Efficient algorithms are considered for the computation of a reduced-order model based on the proper orthogonal decomposition methodology for the solution of parameterized elliptic partial differential equations. The method relies on partitioning the parameter space into subdomains based on the properties of the solution space and then forming a reduced basis for each of the subdomains. This yields more efficient offline and online stages for the proper orthogonal decomposition method. We extend these ideas for inexpensive adjoint based a posteriori error estimation of both the expensive finite element method solutions and the reduced-order model solutions, for a single and multiple quantities of interest. Various numerical results indicate the efficacy of the approach. Copyright © 0000 John Wiley & Sons, Ltd.

Received . . .

KEY WORDS: Error estimation, reduced-order modeling, a posteriori analysis, quantity of interest, proper orthogonal decomposition.

1. INTRODUCTION

We investigate efficient algorithms for the computation of a reduced-order model (ROM) and a posteriori error estimation strategies for the numerical solution of the parameterized nonlinear convection-diffusion-reaction problem,

$$\begin{cases} -\nabla \cdot \epsilon_\mu(\mathbf{x})\nabla u_\mu(\mathbf{x}) + b_\mu(\mathbf{x}) \cdot \nabla u_\mu = f_\mu(u_\mu, \mathbf{x}), & \mathbf{x} \in \Omega, \\ u_\mu(\mathbf{x}) = 0, & \mathbf{x} \in \partial\Omega. \end{cases} \tag{1}$$

Here $\Omega \subset \mathbb{R}^d$ ($d = 2$ or 3) and ϵ_μ, b_μ, and f_μ may depend on the parameter vector $\boldsymbol{\mu}$ in a bounded domain $\mathcal{D} \subset \mathbb{R}^p$. We consider the problem with ϵ_μ Lipschitz and symmetric positive definite, b_μ divergence free and f_μ Lipschitz for all values of $\boldsymbol{\mu} \in \mathcal{D}$. The function f_μ may be nonlinear. The methods presented in this article also apply for nonlinear diffusion, that is if the diffusion coefficient $\epsilon_\mu(\mathbf{x}, u_\mu)$ depends on u_μ. However, we avoid the issues related to the well posedness of such problems here. A numerical example considering this case is explored in §6.2.

The goal of the computation is to approximate the value of a quantity of interest (QoI) of the form

$$Q(u_\mu) = \int_\Omega \psi\, u_\mu \, dx = (\psi, u_\mu) \tag{2}$$

*Correspondence to: Email: estep@stat.colostate.edu

Prepared using nmeauth.cls *[Version: 2010/05/13 v3.00]*

for a given $\psi \in L_2(\Omega)$. The QoI in (2) is a linear functional of the solution u_μ. Nonlinear QoIs require special treatment, and are often dealt by linearization of the QoI [1, 2].

In this article we focus on the reduced modeling approach [3, 4, 5, 6, 7], in particular on proper orthogonal decomposition (POD) [8, 9, 10, 11, 12]. POD techniques form a reduced-order model through expressing a solution in terms of a truncated spectral basis having a dimension much lower than the actual solution space for, say, finite element approximations. Then, approximate solutions belonging to the low-dimensional reduced basis are determined, most usually, through a Galerkin projection. We extend the classical POD algorithm which forms a single spectral basis to a hierarchical approach which forms multiple spectral bases adapted to the parameter dependence.

POD techniques have been applied to numerous science and engineering applications [13, 14, 15, 16, 17, 18, 19]. They often have good approximation properties [20, 21] and are naturally applied to nonaffine and nonlinear problems [22]. However, reduced basis methods for the solution of parameterized PDEs based on POD are not without their drawbacks [22]. POD techniques form the reduced basis by sampling the parameter domain and then computing the full-order model (FOM) solutions, called snapshots. Generally, a large number of sample points, and hence a large number of FOM solves, are performed to ensure that the entire range of solution behavior is captured. However, many of the FOM solutions may contribute only marginally towards the accuracy of the ROM solution, resulting in wasted computational effort. Further, a large dense eigenvalue matrix problem, with dimension equal to the number of sample points, needs to be solved in forming the reduced basis. Moreover, even after the reduced basis has been formed, the cost of assembling a stiffness matrix corresponding to the reduced basis may be unacceptably high if the decay of the eigenvalues is slow. This is because the truncation of the spectral basis is carried out based on the decay of the eigenvalues. Finally, to the best of our knowledge, no a posteriori error estimation based on adjoint problems and computable residuals for QoIs computed from numerical solutions obtained from POD techniques has been carried out. There has been recent work on a posteriori analysis using an optimization approach applied to global norms, see [23].

In this article, we aim to address the drawbacks of POD techniques mentioned above. In particular, we propose a sampling strategy which starts out with a crude sampling, then samples different regions of the parameter domain adaptively. This reduces the size of eigenvalue problem to be solved and also samples in regions where more information is needed to form accurate ROM solutions. Moreover, a hierarchical reduced basis is formed, enabling the formation of the ROM solution more efficiently than standard POD techniques. Finally, we carry out a posteriori error analysis of the ROM solution obtained from POD techniques. The standard a posteriori analysis for reduced basis techniques bounds the error between the ROM solution and the FOM solution [24]. Such bounds are not true error estimates, as the FOM solution is also computed numerically, and hence may have a large error itself. This is important in the context of multiscale, multiphysics problems which necessitate complex solutions techniques and thus have significant numerical error, even for the FOM solutions [25]. As opposed to the previous a posteriori analysis, we derive representations for the error in the QoI between the true continuum solution and the ROM solution. Further, we develop techniques for cheap a posteriori analysis for FOM solutions using POD techniques for computing the error estimate. This in important in situations where the ROM solution has error beyond the specified tolerance, and computing a FOM solution in unavoidable.

The a posteriori error analysis in this article is carried out using variational analysis, computable residuals and adjoint problems. Such a posteriori error estimates are widely used for finite element methods [26, 27, 28]. The strategy relies on computing an adjoint solution based on the adjoint operator corresponding to (1). The key insight that makes error analysis using ROM efficient lies in the observation that the error in the solution, due to its subtractive nature, is a lower dimensional entity than the solution itself. Further, QoIs are lower dimensional quantities as well, and hence this allows employing ROM for the adjoint solutions an attractive option, as we expect the adjoint solution space to be lower dimensional than that of the PDE. Quite often there are multiple QoIs that need to evaluated. The classical analysis of such systems require an adjoint solution for the QoI, and hence is quite expensive. We extend our ideas for using ROM for the adjoint solutions by

DOI: 10.1002/nme

treating the QoI as a parameter in the adjoint problem. This allows inexpensive computation of error estimates for multiples QoIs for both FOM solutions as well as solutions obtained using ROM.

There are other alternatives to the POD approach, e.g., greedy algorithms [24, 6, 12]. The greedy algorithms construct the reduced basis space by adding one basis vector at every step. This new basis vector is chosen as the one which exhibits the largest a posteriori error bound between the solution computed from existing basis and a FOM solution. On the other hand, the POD algorithms construct the entire reduced basis space, which typically involves solving a large eigenvalue problem. Thus the POD basis are often more expensive to construct, though, we try to address the issue of solving large eigenvalue problems by employing a hierarchical algorithm as mentioned earlier. We restrict our algorithms to the POD techniques as greedy algorithms are tailored towards affine linear problems, though there are extensions to nonlinear problems as well [29].

The hierarchical approach proposed is similar to the "h"-type reduced basis methods based on the greedy strategy [30]. However, there are substantial differences in how we sample the domain and form the hierarchical basis. There are also similarities to the recently introduced adaptive basis splitting methods [31]. That method is focused on enriching the reduced basis in the online stage, whereas our focus is on forming the hierarchical basis in the offline stage. Another method to construct POD basis efficiently based on interpolation and notions from differential geometry is considered in [32]. The main focus of that method is to interpolate between existing POD basis, whereas we focus on forming hierarchical basis for the entire parameter space. Another approach for constructing local POD basis for a system of ordinary differential equations is presented in [33]. Their method is based on contiguous partitioning of the state space, whereas in our method local basis are attached to non-contiguous regions in the parameter space. Moreover, our method has a hierarchy of reduced basis whereas the method in [33] partitions the state space only once.

The paper is organized as follows. In §2 we review the basic POD methodology. We introduce our hierarchical POD algorithms in §3. We perform a posteriori analysis to quantify error in the FOM and ROM solutions using POD techniques to compute the adjoint solution in §4. We extend these ideas to treat multiple QoIs in §5. Some additional numerical examples are presented in §6.

2. REVIEW OF CLASSICAL POD

POD techniques reduce the dimension of a system by transforming the original variables onto a new set of uncorrelated variables such that the total norm of the spectrum present in all of the original variables is captured well by a few of the uncorrelated variables [22]. This spectral decomposition allows construction of a reduced basis in which the solution is sought. We employ the method of snapshots [8] to form the ROM model of the parameterized PDE (1). Snapshots refer to the solution of the PDE (1) at a set of sample points.

2.1. Finite element approximation

In a practical setting, the exact solution to (1) is not available and needs to be approximated, which we assume is carried out by a finite element method (FEM). The FEM approximation of the solution of (1) is given by $U_\mu \in V^p$ satisfying

$$(\epsilon_\mu \nabla U_\mu, \nabla v) + (b_\mu \cdot \nabla U_\mu, v) = (f_\mu(U_\mu), v) \quad \forall v \in V_h^p, \tag{3}$$

where $V_h \subset H_0^1(\Omega)$ denotes the standard space of continuous piecewise polynomials of order p and $(\cdot, \cdot)$ denotes the standard $L_2(\Omega)$ inner product.

2.2. Formation of POD reduced basis

Let $\Theta \equiv \{\boldsymbol{\mu}_k, k = 1, \cdots, K\}$ be a sampling of $\mathcal{D}$ and denote the corresponding FEM solutions or snapshots by $\{U_k = U_{\mu_k}, k = 1, \ldots, K\}$. POD computes a reduced basis of dimension $M \ll$

DOI: 10.1002/nme

$\dim(V_h^p)$ as the solution to the optimization problem

$$\{w_i, i = 1, \cdots, M\} = \arg\min \frac{1}{K} \sum_{j=1}^{K} \left\| U_j - \sum_{i=1}^{M} (U_j, w_i)_X w_i \right\|_X^2. \tag{4}$$

Here $(\cdot,\cdot)_X$ and $\|\cdot\|_X$ with $X = 0$ and 1 respectively denote the L^2 and H^1 inner product and norm. The reduced basis vectors w_i are determined by computing the SVD of the matrix having columns U_j or, equivalently, determining the eigenvalues and eigenvectors of the correlation matrix C having entries

$$C_{ij} = \frac{1}{K}(U_j, U_i)_X. \tag{5}$$

Let $\lambda_1 \geq \cdots \geq \lambda_d > 0$ denote the positive eigenvalues of C which, without loss of generality, can be ordered; also let $v_1, \ldots, v_d$ denote the associated eigenvectors. Then the ith POD basis vector is given by

$$w_i = \frac{1}{\sqrt{K\lambda_k}} \sum_{j=1}^{K} (v_i)_j U_j, \tag{6}$$

where $(v_i)_j$ denotes the jth component of the vector v_i. The dimension M of the reduced basis (RB) space may be specified, or chosen using some criteria. One such criteria is to choose a tolerance TOL and then choosing M to be the smallest integer such that

$$K \sum_{i=M+1}^{K} \lambda_i < TOL. \tag{7}$$

Alternately, one can choose M to be the smallest integer such that

$$\frac{\sum_{i=1}^{M} \lambda_i}{\sum_{i=1}^{K} \lambda_i} > FRAC, \tag{8}$$

where $FRAC$ is chosen close to 1 [34]. These criteria are based on the observation that often the first few POD vectors capture most of the energy of the system.

2.3. POD approximations

Let W denote the reduced basis space $\{w_i, i = 1, \ldots, M\}$. Then, for any $\mu \in \mathcal{D}$, the ROM or POD approximation of the solution of (1) is given by $\tilde{U}_\mu$ satisfying

$$(\epsilon_\mu \nabla \tilde{U}_\mu, \nabla v) + (b_\mu \cdot \nabla \tilde{U}_\mu, v) = (f_\mu(\tilde{U}_\mu), v) \quad \forall v \in W. \tag{9}$$

2.4. Offline and online stages

Computing the ROM approximation has an *offline* and an *online* stage; the former is effected a single time whereas the latter may be repeated many times. As a result, one is more willing to incur a greater cost in the offline stage because it can be amortized over the many repetitions of the online stage. On the other hand, because it is repeated many times, one would want the online stage to be significantly less expensive to be effective. The reduced basis $\{w_i, i = 1, \ldots, M\}$ is formed in the offline stage. This involves determining FEM approximations at all K sample points and then solving a $K \times K$ eigenvalue problem; this process can be expensive for large K. In the online stage, the ROM approximation (9) is determined. If M is not too large, this can be inexpensive to accomplish.

Prepared using nmeauth.cls
DOI: 10.1002/nme

3. SAMPLING OF THE PARAMETER DOMAIN AND HIERARCHICAL PROPER ORTHOGONAL DECOMPOSITION

3.1. Parameter sampling strategy

In this section we outline the selective sampling of the parameter domain. We start with a coarse sampling of K points in the parameter domain. Because the sampling is coarse, we do not expect the snapshots to capture all possible behaviors of the PDE, and hence we need to sample additional points in the parameter domain. This is carried out by grouping samples which are correlated into subdomains (see §3.4), and then populating those subdomains so that the number of samples in each subdomain is again K. This process is then carried out for each subdomain till the parameter domain is effectively sampled.

Secondly, a local reduced basis is formed for each subdomain, forming the hierarchical reduced basis method. In classical POD, the solution may require a large number of reduced basis vectors to achieve high accuracy, negating the main advantage of using ROM. The hierarchical reduced basis method forms accurate solutions with relatively few basis vectors. The subdomains are structured as a tree. The details of the algorithm are described below.

3.2. Tree-based structure

The basic structure of the hierarchical basis is a tree-like partition of the parameter domain with a reduced basis space attached to each node. The root node of the tree corresponds to the entire parameter domain, $\mathcal{D} = \mathcal{D}^{(0)}$. This is partitioned into $P^{(0)}$ children subdomains $\mathcal{D}^{(0,i)}, i = 1, \ldots, P^{(0)}$. Then each subdomain $\mathcal{D}^{(0,i)}$ may be further partitioned into $P^{(0,i)}$ subdomains $\mathcal{D}^{(0,i,j)}, j = 1, \ldots, P^{(0,i)}$, and the process continued till some stopping criteria is met. A typical subdomain is identified as $\mathcal{D}^{\tau_l}$ where τ_l is an $l+1$-tuple of the form $(0, i_1, \ldots, i_l)$. It is possible for two leaf nodes in the tree to be at different levels, with the root node being at level 0, its children at level 1 and so forth. This is illustrated in Figure 1.

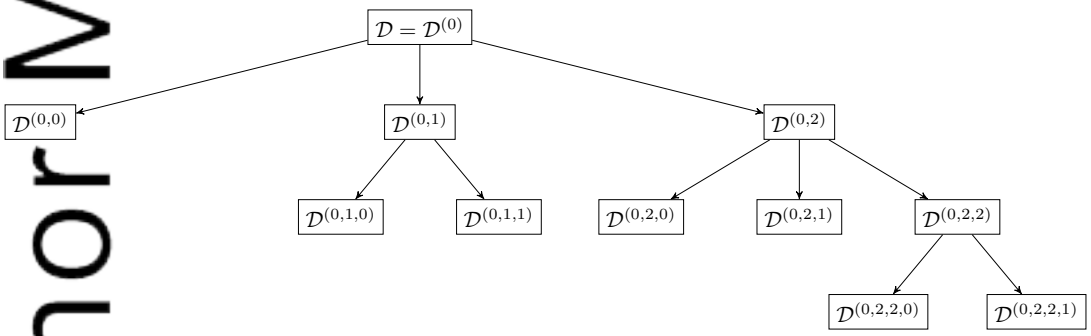

Figure 1. Hierarchical partitioning of the parameter domain.

Next we address the particulars of how a subdomain is represented, partitioned and sampled.

3.3. Subdomain representation

A subdomain is defined by a subset of sampled parameter values of their parent node. We explain this for the subdomains corresponding to the children of the root node $\mathcal{D}$. Let $\mu_1, \ldots, \mu_K$ be parameters in the sampling of $\mathcal{D}$. The K parameters are identified together into $P^{(0)}$ sets denoted as $\Xi^{(0,i)}$ (as described in the next section). Then the ith subdomain, $1 \leq i \leq P^{(0)}$, $\mathcal{D}^{(0,i)}$, is defined implicitly by the parameter set $\Xi^{(0,i)}$. Given an arbitrary $\mu \in \mathcal{D}$, the subdomain to which μ belongs is found by first finding the minimum μ_k such that

$$\mu_k = \underset{1 \leq l \leq K}{\arg\min} \|g(\mu) - g(\mu_l)\|, \tag{10}$$

DOI: 10.1002/nme

where g is a function of μ and $\|\cdot\|$ is the Euclidean norm. Then μ is identified with the jth subdomain such that $\mu_k \in \Xi^{(0,j)}$.

The process described above is repeated for all $\mathcal{D}^{\tau_l}$ that have children, and is terminated when a leaf node is reached. This leaf node represents the subdomain to which the parameter belongs. The function g may be chosen in multiple ways. The simplest option is to choose g as the identity function, $g(\mu) = \mu$. Then (10) represents the Euclidean distance between the parameters. Another options is to choose $g(\mu) = \alpha = [\alpha_1, \ldots, \alpha_{M_2}]$ where α_i are the (spectral) coefficients of the reduced basis corresponding to a ROM solution of dimension M_2. That is, the α_i are obtained from $\tilde{U}_\mu = \sum_{i=1}^{M_2} \alpha_i \psi_i$. This involves solving a POD problem. However, if M_2 is small, this is inexpensive.

3.4. Partitioning of a subdomain

This section explains the process of forming the sets $\Xi^{(0,i)}$, and hence the subdomains $\mathcal{D}^{(0,i)}$, for the root node, $\mathcal{D}$. We assume that there are K parameter values in the sampling of the root node. The k-means clustering algorithm is widely used for clustering algorithms and we employ it here to identify points into the same subdomain [35]. The clustering algorithm is initialized using the k-means++ variant of the algorithm, which often is a more robust approach than random initialization [36]. Pearson's correlation coefficient is used as the "distance" measure in the k-means algorithm. Given two vectors $X^{(j)}$ and $X^{(k)}$, $j \neq k$, of length N, the Pearson's correlation coefficient is defined as,

$$r_{j,k} = \frac{\sum_{i=1}^{N}(X_i^{(j)} - \bar{X^{(j)}})(X_i^{(k)} - \bar{X}^{(k)})}{\sqrt{\sum_{i=1}^{N}(X_i^{(j)} - \bar{X}^{(j)})^2}\sqrt{\sum_{i=1}^{N}(X_i^{(k)} - \bar{X}^{(k)})^2}}, \tag{11}$$

where $X_i^{(j)}$ is the ith component of $X^{(j)}$ and $\bar{X}^{(j)}$ is the mean of the values of $X^{(j)}$.

In the context of POD techniques, the vectors $X^{(j)}$ are formed by the coefficients given in the reduced basis representation of the FEM snapshot U_{μ_j}. That is, given K snapshots U_{μ_j}, we form a reduced basis of dimension M_s where M_s is the number of positive eigenvalues of the correlation matrix C in (5). Then $U_{\mu_j} = \sum_{i=1}^{M_s} \alpha_i \psi_i$ and $X^{(j)} = [\alpha_1, \cdots, \alpha_{M_s}]^\top$. The length of each $X^{(j)}$ is M_s. For each partitioning of a subdomain, the number of child subdomains need to be chosen, which is also the k in the k-means algorithm. There are various heuristics to choose k. In this manuscript, we choose $k = \sqrt{K}$, that is square-root of the number of samples [37]. If this results in a cluster which contains just one sample point, then we reduce k by one, and repeat the process until all clusters contain more than one point.

Finally, it is important to note that a particular partition, $\mathcal{D}_i$, may not be spatially connected (that is, points in $\mathcal{D}_i$ may not be neighbors of each other).

3.5. Subdomain partitioning criteria

A parameter subdomain, $\mathcal{D}^\tau$, is partitioned if two conditions are met:

1. The decay of the largest M_e eigenvalues of the correlation matrix C_{ij} for that subdomain is larger than a specified tolerance, tol_d. That is, if $K\sum_{i=(M_e+1)}^{K} \lambda_i > tol_d$.
2. The minimum value of the correlation coefficients, $r_{j,k}, 1 \leq j,k \leq M_s$, for that subdomain is below a threshold, $mincorr$.

Moreover, the partitioning may be optionally stopped if a node has reached a specified maximum level.

3.6. Sampling the new subdomains and formation of the reduced basis

Once the new subdomains are formed, they need to be sampled, FEM snapshots formed at those sampled values, and reduced basis formed from those snapshots as described in §2. For simplicity, we assume that all subdomains are sampled by K parameters values and the sample set associated

Prepared using nmeauth.cls
DOI: 10.1002/nme

with $\mathcal{D}^{\tau_l}$ is denoted Θ_{τ_l}. For efficiency, we assume the subdomain inherits the parameter values from its parent. For example, the set $\Xi^{(0,i)} \subset \mathcal{D}$ which defines $\mathcal{D}^{(0,1)}$ is also part of its sampling, that is, $\Xi^{(0,i)} \subset \mathcal{D}^{(0,1)}$. Rejection sampling is used to populate the new subdomains. Given a random parameter μ, we determine the leaf subdomain it belongs to using the process described in §3.3. If the subdomain already has K sampled parameters, then the parameter μ is rejected, otherwise the μ is added to the parameter sample for that subdomain. The process repeated until all subdomains have K sampled parameters.

3.7. Offline and online Stages

The subdomain tree and the reduced basis are constructed in the "Offline" stage. Note that the reduced basis spaces corresponding to only the leaf nodes need to be saved. In the "Online" stage, given a parameter value μ, we locate the subdomain that μ belongs to, as outlined in §3.3. Then we retrieve M basis vectors corresponding to the reduced basis of that subdomain, and form the hierarchical ROM or the hierarchical POD solution as discussed in (9). The Offline stage is summarized in Algorithm 1, whereas the Online stage is summarized in Algorithm 2

Algorithm 1: Hierarchical POD Offline Stage

Insert $\mathcal{D}$ into Subdomain Queue
while *Subdomain Queue is not empty*
  Sample subdomains in Subdomain List (§3.6)
  $\mathcal{D}^{\tau_l}$:= Subdomain at front of Subdomain Queue
  Form FEM snapshots and POD reduced basis for $\mathcal{D}^{\tau_l}$
  if $\mathcal{D}^{\tau_l}$ *is to be partitioned (§3.5)*
    Form children subdomains $\mathcal{D}^{\tau_{l+1}}$ of $\mathcal{D}^{\tau_l}$ (§3.4 and §3.3)
    Insert all newly formed subdomains $\mathcal{D}^{\tau_{l+1}}$ at the end of Subdomain Queue

Algorithm 2: Hierarchical POD Online Stage

Input: μ: Parameter
return: $Q(\tilde{U}_\mu)$: QoI value for hierarchical POD solution

Insert $\mathcal{D}$ into Subdomain Queue
Find leaf sub domain $\mathcal{D}^{\tau_l}$ to which μ belongs (§3.6)
Fetch POD reduced basis space W corresponding to $\mathcal{D}^{\tau_l}$
Compute the POD solution, $\tilde{U}_\mu$, as in (9) and evaluate $Q(\tilde{U}_\mu)$

3.8. Numerical Example

We illustrate the properties of the hierarchical algorithm with a numerical example. We consider a reaction-diffusion-convection problem,

$$\begin{cases} -\nabla \cdot \nabla u + [A\cos(\theta)\,,\, A\sin(\theta)] \cdot \nabla u + u = 10, & x \in \Omega, \\ u = 0 & x \in \partial\Omega. \end{cases} \tag{12}$$

The domain Ω is the unit square $[0,\ 1] \times [0,\ 1]$ and $\mu = [A,\ \theta]$ denotes the random parameter vector. The parameter domain, $\mathcal{D}$ is two dimensional, with $A \in [0,\ 40]$ and $\theta \in [0,\ 2\pi]$. The QoI is

$$Q(u) = \int_\Omega \chi_q u\, dx. \tag{13}$$

where χ_q is the characteristic function of $\Omega_q = [0.05,\quad 0.2] \times [0.3,\quad 0.5]$, that is $\chi_q(x) = 1$ if $x \in \Omega_q$ and $\chi_q(x) = 0$ otherwise. We expect the sensitivity of the QoI to vary with θ. The direction

DOI: 10.1002/nme

of the vector field, $[A\cos(\theta)\ ,\ A\sin(\theta)]$, is shown for $\theta = \pi$ and $\theta = \pi/4$ in Figure 2. The $\theta = \pi$ vector field creates a pseudo-inflow boundary near where the QoI is evaluated, and hence we expect the QoI to have relatively large error for this value of θ. A regular triangular mesh with $20 \times 20 \times 2$ elements is employed and the standard space of continuous piecewise linear polynomials, $\mathbb{P}^1$, is employed to form the FEM snapshots. These numerical parameters were chosen to ensure that the numerical error was not overly large.

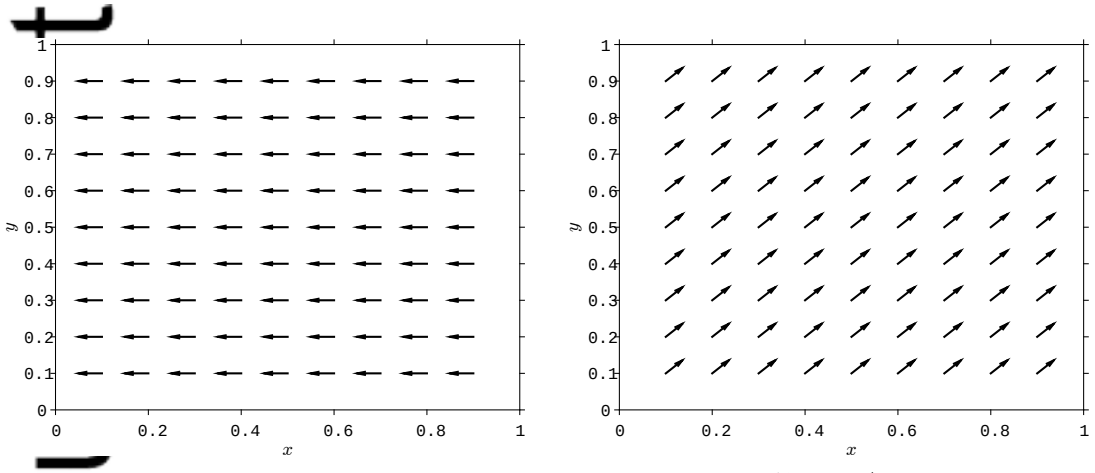

(a) $\theta = \pi$. (b) $\theta = \pi/4$.

Figure 2. Plot of the vector field $[A\cos(\theta),\quad A\sin(\theta)]$.

We compare the "Classical" POD approach with no partitioning with the "Hierarchical" POD approach. For the classical approach, we perform two experiments, with the number of samples for the parameter domain chosen as $K = 40$ and $K = 200$, corresponding to "crude" and "fine" sampling. For the Hierarchical POD, the number of parameter samples for each of the 144 subdomains are $K = 40$ (for a total of randomly sampled 144×40 parameters) while the other numerical parameters used in forming the subdomains are set as $tol_d = 1E-4$, $M_e = 10$, $mincorr = 0.9$ and $g \equiv Id$ where Id denotes the identity function. The subdomains at level 1 ($\mathcal{D}^{(0,i)}$) are illustrated in Figure 3. A particular subdomain may not be connected but have multiple pieces.

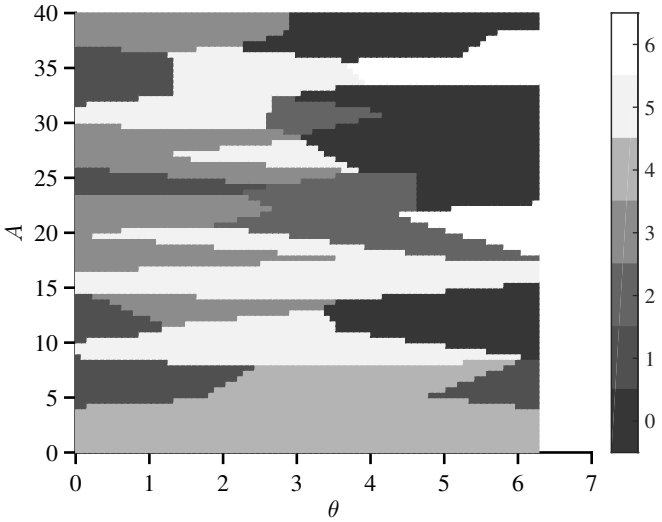

Figure 3. Subdomains at level 1

DOI: 10.1002/nme

We present results for two parameters, $\mu = [\pi,\ 39.8]$ and $\mu = [\pi/4,\ 26.2]$. These parameters are different from the ones that were randomly sampled to form the ROM basis. The $\mu = [\pi,\ 39.8]$ is more difficult as this choice results in a convective vector field $b = [-39.8,\ 0]^\top$, and hence the evaluation of the QoI near the left, pseudo-outflow boundary is challenging. This is also seen from the error in the FEM solutions for the two parameters. The FEM solution for $\mu = [\pi,\ 39.8]$ has an error of -1.6958E-04 whereas the FEM solution for $\mu = [\pi/4,\ 26.2]$ has a much smaller error of 3.5081E-06. The results for different number of basis vectors, M, to form the ROM solution are shown in in Tables I and II for the parameters $\mu = [\pi,\ 39.8]$ and $\mu = [\pi/4,\ 26.2]$ respectively. The values in the tables are the ratio of the POD solution error, $Q(u_\mu - \tilde{U}_\mu)$, to the FEM solution error, $Q(u_\mu - U_\mu)$. As the POD solution approaches the FEM solution in accuracy, the ratio of the POD error and the FEM error approaches one, as seen in the results. The Hierarchical POD techniques are able to form a much an accurate solution with significantly fewer basis vectors in both cases. For the parameter $\mu = [\pi,\ 39.8]$ the Hierarchical solution has the same accuracy with four basis vectors as the Classical techniques have with 18–20 vectors. We observe similar performance for the parameter $\mu = [\pi/4,\ 26.2]$.

M	Classical, $K = 200$	Classical, $K = 40$	Hierarchical, $K = 40$
2	-9.64	4.42	0.69
4	6.50	-6.01	1.17
6	1.59	7.85	1.01
8	2.94	3.09	0.97
10	2.83	3.15	1.00
12	2.65	1.12	1.00
14	1.68	1.35	1.00
16	1.31	1.66	1.00
18	1.20	1.60	1.00
20	1.07	1.12	1.00

Table I. Ratio of the POD error and FEM error in the QoI, $Q(u_\mu - \tilde{U}_\mu)/Q(u_\mu - U_\mu)$, for $\mu = [\pi,\ 39.8]$. As the POD solution approaches the FEM solution in accuracy, the ratio of the POD error and the FEM error approaches one. The POD solutions are computed with M basis vectors using the Classical and the Hierarchical schemes, with the cardinality of the parameter sampling represented as K. The Hierarchical solution was retrieved at level 2. The FEM error is $Q(u_\mu - U_\mu) = -1.6958e-04$.

M	Classical, $K = 200$	Classical, $K = 40$	Hierarchical, $K = 40$
2	436.88	-1456.48	-64.08
4	136.19	563.94	1.02
6	-94.23	-163.57	1.90
8	-8.82	-103.39	2.18
10	-16.75	-37.03	1.02
12	3.65	-3.04	1.01
14	4.05	10.80	0.95
16	7.25	7.05	1.00
18	4.42	4.37	1.00
20	-0.06	1.09	1.00

Table II. Ratio of the POD error and FEM error in the QoI, $Q(u_\mu - \tilde{U}_\mu)/Q(u_\mu - U_\mu)$, for $\mu = [\pi/4,\ 26.2]$. The POD solutions are computed with M basis vectors using the Classical and the Hierarchical schemes, with the cardinality of the parameter sampling represented as K. The Hierarchical solution was retrieved at level 3. The FEM error is $Q(u_\mu - U_\mu) = 3.5081E-06$.

DOI: 10.1002/nme

3.9. Computational Cost

The implicit assumption in forming the Hierarchical POD approach is that we are concerned with efficiency in the Online stage. This is demonstrasted by the numerical example above, and also in the examples in §6. In some cases, Offline cost may also be a concern. However, comparison of the Offline cost for the classical and hierarchical approaches is not straightforward. The hierarchical approach forms a large numbver of samples in order to distinguish different regimes of solution behavior. The classical approach does not take this into account, and hence we cannot directly compare the cost of the Offline costs for the two approaches.

We attempt to compare the sum of Offline and Online costs for the numerical example in §3.8. We observe that for this example the Offline stage of the Hierarchical POD approach involves significantly more FEM solves than the Classical approach, and hence is more computationally demanding in the Offline stage. If the only concern is the speed of the Online stage, then obviously this is not a major issue. Moreover, the increased cost of the Offline stage for the Hierarchical POD is eventually amortized by the speedup obtained using fewer basis vectors in the Online stage. To see this, we define the amortized cost AC_x as,

$$AC_x = \text{Off}_x + \text{On}_x, \tag{14}$$

where $x = C$ or H denotes classical or Hierarchical approaches, Off and On denote the offline and online costs respectively. For the classical approach we define the Offline and Online costs as,

$$\text{Off}_C = (\text{\# Offline Samples}) \times (\text{Cost of FEM solve}) + (\text{Cost to form eigenvalues of correlation matrix}), \tag{15}$$

and

$$\text{On}_C = (\text{\# Online Samples}) \times (\text{Cost of Classical ROM solve}). \tag{16}$$

The corresponding costs for the Hierarchical approach are,

$$\begin{aligned}\text{Off}_H = {} & (\text{\# Offline Samples}) \times (\text{Cost of FEM solve}) + \\ & \text{\# Subdomains} \times (\text{Cost to form eigenvalues of subdomain correlation matrix}),\end{aligned} \tag{17}$$

and

$$\text{On}_H = \text{\# Online Samples} \times [\text{Cost of Hierarchical ROM solve} + \text{Parameter searching cost}]\,. \tag{18}$$

For the numerical example in § 3.8, we compare the costs for Classical approach with total samples $K = 40$ to the Hierarchical approach with number of samples in each subdomain to be $K = 40$ for a total of 144×40 samples. Since the matrices in the FEM solve are sparse, we assume that the cost of a FEM solve is equal to the number of vertices in the mesh, which equals 441 in this case. Moreover, we assume that the cost of forming eigenvalues and eigenvectors from a correlation matrix of size $K \times K$to be K^3. This leads to a cost of 40^3 for the Classical approach, and a cost of 144×40^3 for the Hierarchical approach. Moreover, we assume that, on average, we need 12 vectors to form an accurate ROM solution for the Classical approach. Since the matrices in the Online stage are dense, this leads to a cost of 12^3 per sample. For the Hierarchical approach, we assume we need 4 vectors to form an accurate Online solution. Moreover, we take the parameter searching cost to be $\log 40 \times 3$, which arises from assuming a kd-tree structure [38] to compare parameters in each subdomain, and the average depth for finding a parameter to be 3. The amortized costs for the two approaches are shown in Figure 4. As can be seen, the Classical algorithm has a lower initial cost due to less computationally intensive Offline stage. However, the Hierarchical approach becomes computationally cheaper after around 7000 Online samples.

Finally, as observed in Tables I and II, increasing the sample size of the classical approach from $K = 40$ to $K = 200$ still meant a large number of basis vectors are needed in the Online stage for an accurate solution. In fact, the results for $K = 40$ and $K = 200$ are remarkably similar, indicating that simply increasing the sample size in the Offline stage may not yield an efficiency improvement in the Online stage. This happens as the classical approach, even for the large sample size, forms

Prepared using nmeauth.cls
DOI: 10.1002/nme

a spectral basis that decays slowly as it has to account for a wide range of solution behaviors, whereas the Hierarchical approach is tailored to the characteristics of the solution, and hence is able to form accurate solutions with relatively few basis vectors in the Online stage. We also observe this behavior in Tables VII and VIII in § 6.1. Thus, simply increasing the sample size in the Offline stage of the classical approach may not yield increased efficiency in the Online stage, whereas the hierarchical approach forms accurate solutions with relatively few basis vectors.

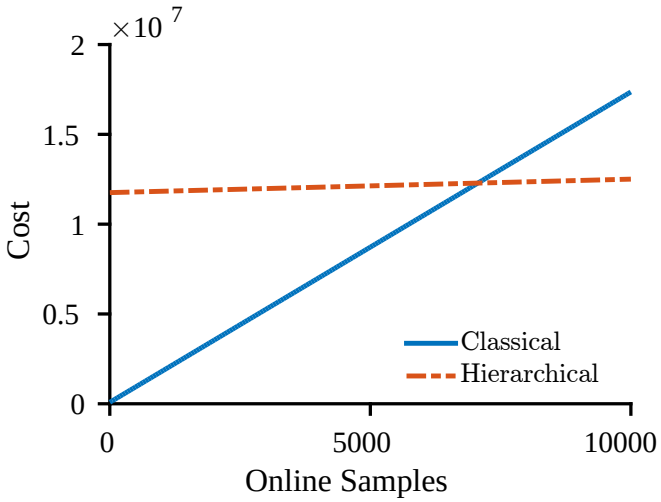

Figure 4. Comparison of Costs for Classical and Hierarchical approaches.

4. A POSTERIORI ERROR ESTIMATION USING HIERARCHICAL POD

We employ adjoint based a posteriori error estimation to quantify the error of numerical solutions. We first review the basic concepts of adjoint based a posteriori error estimation, and then apply our Hierarchical POD algorithm to the adjoint solution computation. This allows the inexpensive and accurate formation of the error estimate, not just for ROM solutions, but higher dimensional FEM solutions as well.

4.1. Adjoint based a posteriori error estimation

The adjoint problem corresponding to the "forward" problem (1) is,

$$-\nabla\cdot\epsilon_\mu\nabla\phi_\mu-(\nabla\cdot b_\mu)\phi_\mu=\overline{f'_\mu(u_\mu,\hat{U}_\mu)}^{\top}\phi_\mu+\psi, \tag{19}$$

where $\overline{f'_\mu(u_\mu,\hat{U}_\mu)},=\int_0^1\frac{\partial f_\mu}{\partial u}(su_\mu+(1-s)\hat{U}_\mu)\,ds$. Here $\hat{U}_\mu$ represents a numerical solution, e.g. the FEM solution $\hat{U}_\mu=U_\mu$ or the POD solution $\hat{U}_\mu=\tilde{U}_\mu$. Standard a posteriori analysis (by integrating (19) with $(u_\mu-\hat{U}_\mu)$, using integration by parts, and using the fact that u_μ satisfies (1)) leads to the error representation,

$$Q(u_\mu-\hat{U}_\mu)=-(\epsilon_\mu\nabla\hat{U}_\mu,\nabla\phi_\mu)-(b_\mu\cdot\nabla\hat{U}_\mu,\phi_\mu)+(f_\mu(\hat{U}_\mu),\phi_\mu) \tag{20}$$

In practice, the adjoint solutions need to be approximated. Let Φ_μ be the FEM solution corresponding to (19). Then the error representation (20) leads to the error estimate,

$$\eta(\hat{U}_\mu):=-(\epsilon_\mu\nabla\hat{U}_\mu,\nabla\Phi_\mu)-(b_\mu\cdot\nabla\hat{U}_\mu,\Phi_\mu)+(f_\mu(\hat{U}_\mu),\Phi_\mu). \tag{21}$$

Another error estimate is obtained by using POD techniques (Classical or Hierarchical) for computing the adjoint solution. Here our conjecture is that the adjoint solutions do not vary greatly

DOI: 10.1002/nme

M	Classical: $K = 200$
5	$-1.1859E-3$
10	$-4.803E-4$
20	$-1.808E-4$
30	$-1.568E-04$
40	$-1.656E-04$
50	$-1.698E-04$

(a) Error in the QoI, $Q(u_\mu - \tilde{U}_\mu)$

$\tilde{M}$	$\tilde{\eta}(U_\mu)$
5	$-2.672E-04$
10	$-1.848E-04$
20	$-1.339E-04$
30	$-1.657E-04$
40	$-1.697E-04$

(b) Performance of the estimate $\tilde{\eta}(U_\mu)$

Table III. Results for $\mu_a = [\pi,\ 39.8]$ for the classical POD algorithm. The error estimate for the FEM solution is $\eta(U_\mu) = -1.696E-04$ and $K = 200$.

as parameter values change. Let $\tilde{\Phi}_\mu$ represent the POD approximation to the adjoint solution. Then this error estimate is,

$$\tilde{\eta}(\hat{U}_\mu) := -(\epsilon_\mu \nabla \hat{U}_\mu, \nabla \tilde{\Phi}_\mu) - (b_\mu \cdot \nabla \hat{U}_\mu, \tilde{\Phi}_\mu) + (f_\mu(\hat{U}_\mu), \tilde{\Phi}_\mu). \tag{22}$$

Given a numerical solution $\hat{U}_\mu$, $\tilde{\eta}(\hat{U}_\mu)$ is significantly less expensive to compute relative to the estimate $\eta(\hat{U}_\mu)$. In this section we explore strategies for computing $\tilde{\Phi}_\mu$ and hence $\tilde{\eta}(\hat{U}_\mu)$ efficiently.

4.2. ROM for error estimation using classical POD

In this section we explore the efficiency of using ROM for adjoint based error estimation, and compare it with the efficiency of using ROM for computing the numerical solutions to (1). Since the error is a much simpler entity than the solution to the PDE itself, we expect to use fewer basis vectors for error estimation as opposed to approximating a QoI. We illustrate this with the example in §3.8 for the classical POD algorithm using $K = 200$ for sampling the parameter domain for the parameter $\mu = [\pi,\ 39.8]$ in Table III . The error in the QoI using different number of basis vectors for the ROM forward solution, $\tilde{U}_\mu$, is shown in Table IIIa. This shows we need around 40 basis vectors for the POD solution to approximate the error of the FEM solution up to two digits of accuracy. Now, we show results for the number of basis vectors, $\tilde{M}$, in the construction of the POD solution, $\tilde{\Phi}_\mu$ for the adjoint equation. The adjoint FEM snapshots, Φ_μ, are approximated in the space of continuous piecewise quadratic polynomials, $\mathbb{P}^2$. We investigate the accuracy of the estimate $\tilde{\eta}(U_\mu)$ by varying $\tilde{M}$ and comparing it with the estimate $\eta(U_\mu)$ computed using the FEM adjoint approximation in Table IIIb. We see we need 30 vectors for an accurate (up to two digits) error estimate, which is 25% less than the number required for the accurate solution $\tilde{U}_\mu$. This example illustrates the potential of using ROM for inexpensive forming error estimates, even for full order FEM solutions.

4.3. Hierarchical ROM for error estimation

In this section, we apply the ideas developed in §3 for approximation of the adjoint solution. That is, a hierarchical ROM for the adjoint solution is formed. We illustrate the efficacy of this approach for the convection-diffusion problem (12) in §3.8. One issue in the construction of the parameter subdomains for the adjoint ROM is whether the partitioning is carried out based on the forward snapshots U_μ or the adjoint snapshots Φ_μ. Since the hierarchical ROM for the forward solutions, U_μ, is already constructed, using the same partitioning for the adjoint ROM saves computational effort. We show the results for partitioning based on both forward snapshots, U_μ, and the adjoint snapshots, Φ_μ, and these strategies are labeled as "Forward Samp." and "Adjoint Samp.". The numerical parameters for the "Forward Samp." are the same as in §3.8. The numerical parameters in the case of "Adjoint Samp." were set as $tol_d = 1E-7$, $M_e = 10$, $mincorr = 0.9$ and $g \equiv Id$ for the construction of the hierarchical ROM for the adjoint PDE.

Table IV shows the effectiveness of the estimate $\tilde{\eta}(U_\mu)$ for the error analysis of the FEM solution U_μ for the parameters $[\pi,\ 39.8]$ and $[\pi/4,\ 26.2]$. The results indicate that we obtain an accurate

DOI: 10.1002/nme

error estimate using just 3 basis vectors for $[\pi,\ 39.8]$ and 1 basis vectors for $[\pi/4,\ 26.2]$ for both the "Forward Samp." and "Adjoint Samp." strategies. Moreover, we again observe that very few basis vectors are needed for accurate error estimate.

Table V shows results for the error analysis of the forward hierarchical POD solutions $\tilde{U}_\mu$. The solutions $\tilde{U}_\mu$ were computed using $M = 4$ basis vectors. We see that we now need three basis vectors for an accurate error estimate for both parameters.

M	Forward Samp.	Adjoint Samp.
1	1.45	1.45
2	0.64	0.68
3	1.09	1.10
4	1.06	1.06
5	0.98	0.99
6	0.98	1.00
7	1.01	1.00
8	1.01	1.00
9	1.00	1.00
10	1.00	1.00
11	1.00	1.00
12	1.00	1.00

(a) $\mu = [\pi,\ 39.8]$, $\eta(U_\mu) = -1.6958E-04$

$\tilde{M}$	Forward Samp.	Adjoint Samp.
1	1.03	1.18
2	1.00	0.96
3	1.05	1.00
4	1.00	1.00
5	1.00	1.00
6	1.00	1.00
7	1.00	1.00
8	1.00	1.00
9	1.00	1.00
10	1.00	1.00
11	1.00	1.00
12	1.00	1.00

(b) $\mu = [\pi/4,\ 26.2]$, $\eta(U_\mu) = 3.5081E-06$

Table IV. Values of the ratio $\tilde{\eta}(U_\mu)/\eta(U_\mu)$.

M	Forward Samp.	Adjoint Samp.
1	1.83	1.83
2	0.66	0.69
3	1.08	1.08
4	1.04	1.02
5	0.97	0.97
6	0.97	1.00
7	1.01	1.00
8	1.01	1.00
9	1.00	1.00
10	1.00	1.00
11	1.00	1.00
12	1.00	1.00

(a) $\mu = [\pi,\ 39.8]$, $\eta(\tilde{U}_\mu) = -1.9809E-04$

$\tilde{M}$	Forward Samp.	Adjoint Samp.
1	0.92	0.72
2	0.93	0.87
3	0.99	1.02
4	1.00	1.02
5	1.00	1.00
6	1.00	1.00
7	1.00	1.01
8	1.00	1.00
9	1.00	1.00
10	1.00	1.00
11	1.00	1.00
12	1.00	1.00

(b) $\mu = [\pi/4,\ 26.2]$, $\eta(\tilde{U}_\mu) = 3.5818E-06$

Table V. Values of the ratio $\tilde{\eta}(\tilde{U}_\mu)/\eta(\tilde{U}_\mu)$. The solutions $\tilde{U}_\mu$ were computed using $M = 4$ basis vectors.

5. HIERARCHICAL ROM FOR ERROR ESTIMATION OF MULTIPLE QOIS

Quite often multiple QoIs need to be evaluated, and this makes adjoint based error analysis significantly expensive as a separate adjoint problem needs to be solved for each QoI. However, we apply the ideas developed for error estimation using hierarchical POD for the case of multiple parameterized QoIs. That is, the QoIs are represented as,

$$Q(u_\mu) = (\psi_{\hat{\mu}}, u_\mu), \tag{23}$$

DOI: 10.1002/nme

where $\hat{\mu} \in \hat{\mathcal{D}}$ is the parameter defining the function $\psi_{\hat{\mu}}$. The adjoint equation becomes,

$$-\nabla \cdot \epsilon_\mu \nabla \phi_{\tilde{\mu}} - (\nabla \cdot b_\mu)\phi_{\tilde{\mu}} = \overline{f'_\mu(u_\mu, \hat{U}_\mu)}^\top \phi_{\tilde{\mu}} + \psi_{\hat{\mu}}. \tag{24}$$

That is, the adjoint equation has two parameters now, μ and $\hat{\mu}$. In forming the hierarchical POD for the adjoint solution, we consider these as one parameter, $\tilde{\mu} = [\mu, \hat{\mu}] \in \mathcal{D} \times \hat{\mathcal{D}}$. Now the partitioning of the parameter space is carried out using the adjoint snapshots $\Phi_{\tilde{\mu}}$, as the forward solutions $\hat{U}_\mu$ do not account for the parameter $\hat{\mu}$.

5.1. Example

We illustrate the above scheme for the convection diffusion example is §3.8. The parameterized QoI is now defined as,

$$Q(u) = \int_\Omega \psi_{\hat{\mu}}\, u\, dx, \tag{25}$$

where $\hat{\mu} = [a, b, c]$, $\psi_{\hat{\mu}} = 100x^2(1-x)^2(\exp(a(x-b)^2) - c)y^2(1-y)^2, 0.1 < a < 10, 0 < b < 1$ and $-10 < c < 10$. The parameter space corresponding to the parameterized QoI, $\hat{\mathcal{D}}$, is three-dimensional. Line-plots of $\psi_{\hat{\mu}}$ along the $x-$axis for two parameters, $\hat{\mu} = [10.0,\ 1.0,\ 10]$ and $\hat{\mu} = [4.0,\ 0.1,\ 10.0]$ are shown in Figures 5a and 5b.

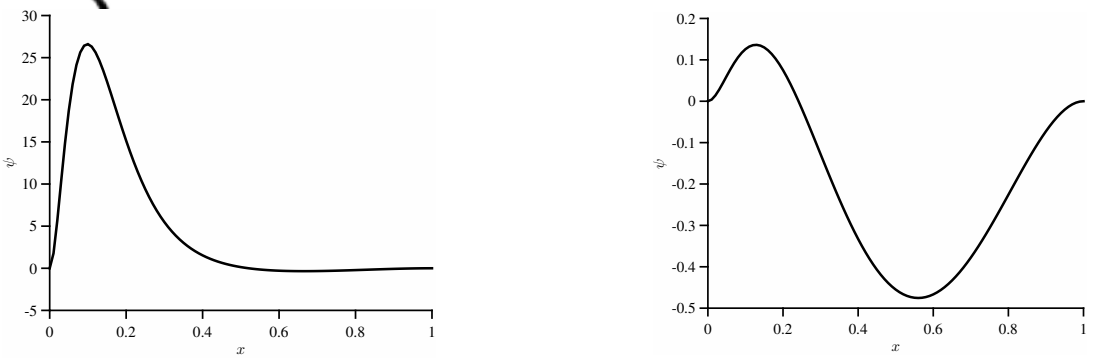

(a) $\hat{\mu} = [10.0,\ 1.0,\ 10]$ (b) $\hat{\mu} = [4.0,\ 0.1,\ 10.0]$

Figure 5. Line plots of $\psi_{\hat{\mu}}$ along the $x-$axis.

For simplicity, we only consider the effect of employing ROM for the adjoint PDE to quantify the error in various QoIs for a particular FEM solution of (12). This particular FEM solution is computed with $A = 30$ and $\theta = \pi$. The numerical parameters for Hierarchical POD for the adjoint PDE are set as $K = 40$, $tol_d = 1E-7$, $M_e = 5$, $mincorr = 0.9$ and $g \equiv Id$. The FEM adjoint problem has 14841 degrees of freedom and for each QoI a different adjoint problem needs to be solved. This is quite expensive if FEM adjoint solutions are used for error estimation.

However, we show results for error estimates computed using Hierarchical ROM in Table VI. The estimators $\eta_{\hat{\mu}}$ and $\tilde{\eta}_{\hat{\mu}}$, refer to the estimated error in the QoIs using the FEM adjoint solution and hierarchical ROM adjoint solutions respectively. We observe that the error estimate using the Hierarchical ROM for adjoint is almost as accurate as the error estimate obtained using the FEM adjoint solution using only 6 basis vectors for $[10.0,\ 1.0,\ 10]$ and 4 for $[4.0,\ 0.1,\ 10.0]$, hence yielding significant savings in computational effort.

6. NUMERICAL EXAMPLES

In this section we investigate the hierarchical POD ideas on two more examples. The results are illustrated for some chosen parameters μ, which are different from the randomly sampled parameters used to form the ROM basis.

DOI: 10.1002/nme

$\tilde{M}$	$\tilde{\eta}_{\hat{\mu}}(U_\mu)/\eta_{\hat{\mu}}(U_\mu)$
1	0.00
2	0.01
3	0.47
4	0.65
5	0.90
6	0.98
7	1.02
8	1.02
9	1.01
10	1.01

(a) $\hat{\mu} = [10.0,\ 1.0,\ 10]$, $\eta(U_\mu) = 4.3E-2$

$\tilde{M}$	$\tilde{\eta}_{\hat{\mu}}(U_\mu)_{\hat{\mu}}/\eta(U_\mu)$
1	0.24
2	0.53
3	1.25
4	1.02
5	0.99
6	1.00
7	1.00
8	1.00
9	1.00
10	1.00

(b) $\mu = [4.0,\ 0.1,\ 10.0]$, $\eta_{\hat{\mu}}(U_\mu) = 1.7715E-04$

Table VI. Values of the ratio $\tilde{\eta}_{\hat{\mu}}(U_\mu)/\eta_{\hat{\mu}}(U_\mu)$.

6.1. Poisson Problem

Consider the Poisson problem [24],

$$\begin{cases} \nabla \cdot \epsilon(\mathbf{x}) \nabla u = 0 & \mathbf{x} \in \Omega, \\ u = 0, & \mathbf{x} \in \Gamma_d, \\ \frac{\partial u}{\partial n} = 0, & \mathbf{x} \in \Gamma_n, \\ \frac{\partial u}{\partial n} = 1, & \mathbf{x} \in \Gamma_o. \end{cases} \tag{26}$$

where Ω is the unit square $[0,\ 1] \times [0,\ 1]$, Γ_o is the lower boundary, $y = 0$, and Γ_d is the top boundary, $y = 1$ and $\Gamma_n = \partial\Omega \backslash (\Gamma_o \cup \Gamma_d)$. The diffusion coefficient, $\epsilon(x)$, is piecewise constant, as shown in Figure 6. Here each $\epsilon_i \in [0.1, 10]$ for $i = 1, \cdots, 3$. That is, our parameter space is 3-dimensional, $\mathcal{D} = [0.1,\ 10]^3$. The value of the ϵ in the top right is set as 1. The QoI is,

$$Q(u) = \int_\Omega \chi_q u \, dx. \tag{27}$$

where χ_q is the characteristic function of $\Omega_q = [0.0625,\ 0.25] \times [0.0625,\ 0.25]$.

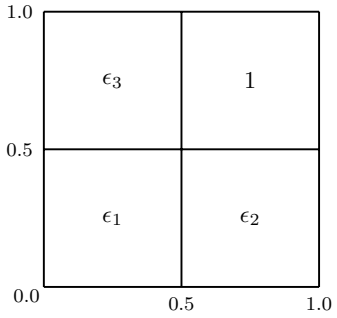

Figure 6. Diffusion Coefficient, $\epsilon(x)$, is piecewise constant.

The FEM problems corresponding to the forward problem (26) were solved on a regular triangular mesh of $16 \times 16 \times 2$ triangular elements whereas the adjoint solutions were solved on a a regular triangular mesh of $32 \times 32 \times 2$ triangular elements. These meshes gave reasonably accurate FEM solution, while also ensuring that the elements align with the boundaries where the diffusion coefficient jumps. Standard space of continuous piecewise linear polynomials, $\mathbb{P}^1$ is employed to form the FEM snapshots for (28) whereas the adjoint FEM snapshots Φ_μ are approximated on the space of continuous piecewise quadratic polynomials, $\mathbb{P}^2$. The numerical parameters are set as

DOI: 10.1002/nme

$tol_d = 1E-7$, $M_e = 10$, $mincorr = 0.9$ and $g \equiv Id$. Further, the max-level of the tree is set at three.

We show results for two parameters. The first parameter is $[10.0,\ 0.1,\ 0.1]$, which has large jumps in the diffusion coefficient, and hence is a relatively hard problem. The second parameter is arbitrarily chosen as $[2.6,\ 2.1,\ 3.2]$, representing an easier problem. The FEM solution for $\mu = [10.0,\ 0.1,\ 0.1]$ has two orders of magnitude greater error (FEM error = $6.595e-04$) than the solution corresponding to $\mu = [2.6,\ 2.1,\ 3.2]$ (FEM error = $6.601e-06$), indicating the relatively difficult nature of the first problem. The results for the ratio of POD error and the FEM error in the QoI, $Q(u_\mu - \tilde{U}_\mu)/Q(u_\mu - U_\mu)$, for different number of basis vectors, M, to form the POD solution are shown in Tables VII and VIII for the parameters $\mu = [10.0,\ 0.1,\ 0.1]$ and $\mu = [2.0,\ 3.0,\ 4.0]$ respectively. The Classical POD solution is computed with $K = 80$ and $K = 800$, corresponding to the "crude" and "fine" sampling of the parameter domain. The Hierarchical POD solution is computed with $K = 80$ for each subdomain. We observe that the Hierarchical ROM solutions have significantly lower error than the Classical ROM solutions for low value of M, indicating the efficiency of this approach. This is especially apparent for the harder problem corresponding to $\mu = [10.0,\ 0.1,\ 0.1]$.

M	Classical, $K = 800$	Classical, $K = 80$	Hierarchical, $K = 80$
1	7.62	7.93	1.00
2	5.40	8.25	2.01
3	5.26	4.59	1.03
4	3.54	4.63	1.01
5	3.33	3.57	1.00
6	1.38	3.12	1.00
7	1.25	1.48	1.00
8	1.05	1.37	1.00
9	1.00	1.02	1.00
10	1.00	1.01	1.00

Table VII. Ratio of the POD error and FEM error in the QoI, $Q(u_\mu - \tilde{U}_\mu)/Q(u_\mu - U_\mu)$, for $\mu = [10.0,\ 0.1,\ 0.1]$. The POD solutions are computed with M basis vectors using the Classical and the Hierarchical schemes, with the cardinality of the parameter sampling represented as K. The FEM error is $Q(u_\mu - U_\mu) = 7.577E-03$.

M	Classical, $K = 800$	Classical, $K = 80$	Hierarchical, $K = 80$
1	54.12	63.25	30.54
2	-1.56	-8.85	11.75
3	-10.59	-11.68	-2.61
4	-4.28	-7.54	-0.62
5	0.71	0.27	0.18
6	0.84	1.04	1.11
7	0.85	1.00	0.99
8	0.93	0.94	1.00
9	0.93	0.95	1.00
10	1.00	1.00	1.00

Table VIII. Ratio of the POD error and FEM error in the QoI, $Q(u_\mu - \tilde{U}_\mu)/Q(u_\mu - U_\mu)$, for $\mu = [2.0,\ 3.0,\ 4.0]$. The POD solutions are computed with M basis vectors using the Classical and the Hierarchical schemes, with the cardinality of the parameter sampling represented as K. The FEM error is $Q(u_\mu - U_\mu) = 2.978E-05$.

Table IX shows the effectiveness of the estimate $\tilde{\eta}(U_\mu)$ for the error analysis of the FEM solution. The results indicate that we obtain an accurate error estimate using very few basis vectors. Table X shows similar results for the error analysis of the forward hierarchical POD solutions $\tilde{U}_\mu$.

Prepared using nmeauth.cls
DOI: 10.1002/nme

$\tilde{M}$	$\tilde{\eta}(U_\mu)/\eta(U_\mu)$
1	0.42
2	0.85
3	0.86
4	0.95
5	0.99
6	0.99
7	1.00

(a) $\mu = [10.0, 0.1, 0.1]$, $\eta(U_\mu) = 7.577E-03$

$\tilde{M}$	$\tilde{\eta}(U_\mu)/\eta(U_\mu)$
1	0.51
2	0.81
3	1.03
4	1.03
5	1.00
6	0.99
7	1.01

(b) $\mu = [2.0, 3.0, 4.0]$, $\eta(U_\mu) = 2.978E-05$

Table IX. Values of the ratio $\tilde{\eta}(U_\mu)/\eta(U_\mu)$.

$\tilde{M}$	$\tilde{\eta}(\tilde{U}_\mu)/\eta(\tilde{U}_\mu)$
1	0.42
2	0.85
3	0.85
4	0.95
5	0.99
6	0.99
7	1.00

(a) $\mu = [10.0, 0.1, 0.1]$, $\eta(\tilde{U}_\mu) = 7.579E-03$

$\tilde{M}$	$\tilde{\eta}(\tilde{U}_\mu)/\eta(\tilde{U}_\mu)$
1	0.55
2	0.82
3	1.02
4	1.03
5	1.00
6	0.99
7	1.00

(b) $\mu = [2.0, 3.0, 4.0]$, $\eta(\tilde{U}_\mu) = 3.292E-05$

Table X. Values of the ratio $\tilde{\eta}(\tilde{U}_\mu)/\eta(\tilde{U}_\mu)$. The solutions $\tilde{U}_\mu$ were computed using $M = 6$ basis vectors.

6.2. Nonlinear Example

Consider the nonlinear problem,

$$\begin{cases} -\nabla\cdot(\alpha_1+u^2)\nabla u + \frac{\alpha_2}{\alpha_3}(e^{\alpha_3 u}-1) = 10\sin(2\pi x)\sin(2\pi y), & \mathbf{x} \text{ in } \Omega, \\ u = 0 & \mathbf{x}\in\Gamma_d, \\ \frac{\partial u}{\partial n} = 0 & \mathbf{x}\in\Gamma_n. \end{cases} \tag{28}$$

where Ω is the unit square $[0,\,1]\times[0,\,1]$, Γ_n is the lower boundary, $y=0$, and $\Gamma_d = \partial\Omega\backslash\Gamma_n$. The parameter space, represented by $\mu = [\alpha_1,\alpha_2,\alpha_3] \subset \mathcal{D} \equiv [0.1, 1.0]\times[0.01, 8.0]^2$, is three dimensional. The QoI is,

$$Q(u) = \int_\Omega \psi u\, dx. \tag{29}$$

where $\psi = \rho^{-2}e^{\rho^2/(\rho^2-|\mathbf{x}|^2)}$ approximates the Dirac delta function as $\rho\to 0$. We set $\rho = 0.1$.

The adjoint problem corresponding to (28) is,

$$\begin{cases} -\nabla\cdot\overline{\epsilon(u,U)}\nabla\phi + \overline{\epsilon'(u,U)}\cdot\nabla\phi + \overline{f'(u,U)}\phi = \psi & \\ \phi = 0 & \mathbf{x}\in\Gamma_d, \\ \frac{\partial\phi}{\partial n} = 0 & \mathbf{x}\in\Gamma_n. \end{cases} \tag{30}$$

where

$$\overline{\epsilon(u,U)} = \int_0^1 \alpha_1 + (su+(1-s)U)^2\, ds, \tag{31}$$

$$\overline{\epsilon'(u,U)} = \int_0^1 2(su+(1-s)U)\nabla((su+(1-s)U))\, ds, \tag{32}$$

and

$$\overline{f'(u,U)} = \int_0^1 \alpha_2 e^{\alpha_3(su+(1-s)U)}\, ds. \tag{33}$$

DOI: 10.1002/nme

The definition (30) implies,

$$Q(u-U) = (u-U,\psi) = -((\alpha_1 + U^2)\nabla U, \phi) - (\frac{\alpha_2}{\alpha_3}(e^{\alpha_3 U} - 1), \phi) + 10\sin(2\pi x)\sin(2\pi y). \tag{34}$$

The FEM problems are solved on a regular triangular mesh of $30 \times 30 \times 2$ triangular elements. Standard space of continuous piecewise linear polynomials, $\mathbb{P}^1$ is employed to form the FEM snapshots for (28) whereas the adjoint FEM snapshots Φ_μ are approximated on the space of continuous piecewise quadratic polynomials, $\mathbb{P}^2$. Other values of numerical parameters for the Hierarchical ROM are $K = 40$, $tol_d = 1E-6$, $M_e = 10$, $mincorr = 0.9$ and $g \equiv Id$. Further, the maximum level of the tree is set as three.

The results for $\mu = [1.0, 8.0, 0.1]$ and $\mu = [1.0, 0.01, 8.0]$ are shown in Table. XI. The results highlight how the Hierarchical ROM achieves a more accurate solution using fewer basis vectors compared to Classical ROM.

M	Classical	Hierarchical
2	-2.26	-8.34
4	-4.97	0.76
6	-4.97	2.90
8	6.83	1.09
10	-3.60	1.01
12	-4.53	1.09
14	-3.40	1.04
16	0.93	1.04
18	1.04	1.01
20	0.58	0.98

(a) $\mu = [0.1, 1.0, 8.0]$, $Q(u_\mu - U_\mu) = -7.547E-04$

M	Classical	Hierarchical
2	-1.63	0.37
4	-0.13	1.09
6	1.25	0.94
8	1.07	1.00
10	1.08	1.00
12	0.99	1.00
14	0.99	1.00
16	1.00	1.00
18	1.00	1.00
20	1.00	1.00
22	1.00	1.00

(b) $\mu = [1.0, 0.01, 8.0]$, $Q(u_\mu - U_\mu) = -4.52E-04$

Table XI. Ratio of the POD error and FEM error in the QoI, $Q(u_\mu - \tilde{U}_\mu)/Q(u_\mu - U_\mu)$. The POD solutions are computed with M basis vectors using the Classical and the Hierarchical schemes, with the cardinality of the parameter sampling represented as K.

Now we show results for the error estimate of the FEM solutions, U_μ, using Hierarchical ROM in Table XII. Similar results for the error estimate of the Hierarchical POD solutions, $\tilde{U}_\mu$ in Table XIII. In all cases, the error estimate using the Hierarchical ROM adjoint solution computes an accurate error estimate using a small number of basis vectors.

$\tilde{M}$	$\tilde{\eta}(U_\mu)/\eta(U_\mu)$
1	0.87
2	0.91
3	0.98
4	0.99
5	1.00
6	1.00
7	1.00
8	1.00
9	1.00
10	1.00

(a) $\mu = [0.1, 1.0, 8.0]$, $\eta(U_\mu) = -7.547E-04$

$\tilde{M}$	$\tilde{\eta}(U_\mu)/\eta(U_\mu)$
1	1.05
2	1.00
3	1.00
4	1.00
5	1.00
6	1.00
7	1.00
8	1.00
9	1.00
10	1.00

(b) $\mu = [1.0, 0.01, 8.0]$, $\eta(U_\mu) = -4.520E-04$

Table XII. Values of the ratio $\tilde{\eta}(U_\mu)/\eta(U_\mu)$.

DOI: 10.1002/nme

$\tilde{M}$	$\tilde{\eta}(\tilde{U}_\mu)/\eta(\tilde{U}_\mu)$
1	0.97
2	0.96
3	0.99
4	0.99
5	1.00
6	1.00
7	1.00
8	1.00
9	1.00
10	1.00

(a) $\mu = [0.1, 1.0, 8.0]$, $\eta(\tilde{U}_\mu) = -2.188E-03$

$\tilde{M}$	$\tilde{\eta}(\tilde{U}_\mu)/\eta(\tilde{U}_\mu)$
1	1.05
2	1.00
3	1.00
4	1.00
5	1.00
6	1.00
7	1.00
8	1.00
9	1.00
10	1.00

(b) $\mu = [1.0, 0.01, 8.0]$, $\eta(\tilde{U}_\mu) = -4.227E-04$

Table XIII. Values of the ratio $\tilde{\eta}(\tilde{U}_\mu)/\eta(\tilde{U}_\mu)$. The solutions $\tilde{U}_\mu$ were computed using $M = 6$ basis vectors.

7. CONCLUSIONS

We develop POD based algorithms for efficient solution of parameterized PDEs and a posteriori error estimation. Our hierarchical POD algorithm samples the parameter domain based on the properties of the solution space, instead of uniform random sampling. Moreover, the parameter domain is decomposed into sub-regions based on the solution behavior and a local reduced basis is computed for each sub-region. This allows accurate yet inexpensive computation of solution in the Online stage of the algorithm when computational resources are of vital importance. Our results indicate significant saving of computational effort compared to the standard algorithm for a number of problems.

Reliable use of numerical simulations in science and engineering applications necessitate not just fast computation of the discrete solution, but also quantification of its error. In this regard we extend the hierarchical approach to the computation of the adjoint solutions, hence leading to formation of accurate error estimates in a quantity of interest. Employing ROM for adjoint solutions is also attractive as we expect the adjoint solution space to be of much lower dimensional than the PDE solution space. We see this behavior in the numerical examples where relatively few vectors in the adjoint reduced basis provide a good error estimate. We also extend the idea of ROM for parameterized PDEs to form error estimates for multiple QoIs. The inexpensive error estimation is carried out for not only the ROM solutions but also high dimension FEM solutions. The latter is important in scenarios where computing a ROM solution for a PDE has too large an error so a FEM solution in unavoidable. Employing hierarchical ROM for forming error estimates for multiple QoIs in such a case yields significant savings in the computational budget as it avoids solving FEM adjoint solution multiple times for each QoI.

REFERENCES

1. Heuveline V, Rannacher R. A posteriori error control for finite element approximations of elliptic eigenvalue problems. *Advances in Computational Mathematics* 2001; **15**(1-4).
2. Carey V, Estep D, Tavener S. A posteriori analysis and adaptive error control for multiscale operator decomposition solution of elliptic systems I: Triangular systems. *SIAM Journal on Numerical Analysis* Jan 2009; **47**(1):740–761.
3. Noor AK, Peters JM. Reduced basis technique for nonlinear analysis of structures. *Aiaa journal* 1980; **18**(4):455–462.
4. Prudhomme C, Rovas DV, Veroy K, Machiels L, Maday Y, Patera AT, Turinici G. Reliable real-time solution of parametrized partial differential equations: Reduced-basis output bound methods. *Journal of Fluids Engineering* 2002; **124**(1):70–80.
5. Kunisch K, Volkwein S. Galerkin proper orthogonal decomposition methods for parabolic problems. *Numerische Mathematik* 2001; **90**(1):117–148.
6. Quarteroni A, Rozza G, Manzoni A. Certified reduced basis approximation for parametrized partial differential equations and applications. *Journal of Mathematics in Industry* 2011; **1**(1):1–49.

Prepared using nmeauth.cls
DOI: 10.1002/nme

7. Gunzburger MD. *Finite Element Methods for Viscous Incompressible Flows: A guide to theory, practice, and algorithms*. Elsevier, 2012.
8. Sirovich L. Turbulence and the dynamics of coherent structures, parts i–iii. *Quarterly of applied mathematics* 1987; **45**(3):561–571.
9. Holmes P, Lumley JL, Berkooz G. *Turbulence, coherent structures, dynamical systems and symmetry*. Cambridge university press, 1998.
10. Kunisch K, Volkwein S. Control of the burgers equation by a reduced-order approach using proper orthogonal decomposition. *Journal of Optimization Theory and Applications* 1999; **102**(2):345–371.
11. Afanasiev K, Hinze M. Adaptive control of a wake flow using proper orthogonal decomposition. *Lecture Notes in Pure and Applied Mathematics* 2001; :317–332.
12. Alfio Quarteroni FN Andrea Manzoni. *Reduced Basis Methods for Partial Differential Equations*. Springer International Publishing, 2015. URL `http://www.ebook.de/de/product/25073372/alfio_quarteroni_andrea_manzoni_federico_negri_reduced_basis_methods_for_partial_differential_equations.html`.
13. Gunzburger MD, Peterson JS, Shadid JN. Reduced-order modeling of time-dependent pdes with multiple parameters in the boundary data. *Computer Methods in Applied Mechanics and Engineering* 2007; **196**(4):1030–1047.
14. Burkardt J, Gunzburger M, Lee HC. Pod and cvt-based reduced-order modeling of navier–stokes flows. *Computer Methods in Applied Mechanics and Engineering* 2006; **196**(1):337–355.
15. Hall K, Thomas J, Dowell E. reduced-order modeling of unsteady small-disturbance flows using a frequency-domain proper orthogonal decomposition technique. *identity* 1999; **5**(679):8.
16. Hall KC, Thomas JP, Dowell EH. Proper orthogonal decomposition technique for transonic unsteady aerodynamic flows. *AIAA journal* 2000; **38**(10):1853–1862.
17. Amabili M, Sarkar A, Paıdoussis M. Reduced-order models for nonlinear vibrations of cylindrical shells via the proper orthogonal decomposition method. *Journal of Fluids and Structures* 2003; **18**(2):227–250.
18. Banks H, del Rosario R, Smith R. Reduced order model feedback control design: Computational studies for thin cylindrical shells. *IEEE Trans. Auto. Contr*, Citeseer, 1998.
19. Hömberg D, Volkwein S. *Suboptimal control of laser surface hardening using proper orthogonal decomposition*. WIAS Berlin, 2001.
20. Diwoky F, Volkwein S. Nonlinear boundary control for the heat equation utilizing proper orthogonal decomposition. *Fast Solution of Discretized Optimization Problems*. Springer, 2001; 73–87.
21. Kunisch K, Volkwein S. Galerkin proper orthogonal decomposition methods for a general equation in fluid dynamics. *SIAM Journal on Numerical analysis* 2002; **40**(2):492–515.
22. Manzoni A, Quarteroni A, Rozza G. Computational reduction for parametrized pdes: strategies and applications. *Milan Journal of Mathematics* 2012; **80**(2):283–309.
23. Gubisch M, Neitzel I, Volkwein S. A-posteriori error estimation of discrete pod models for pde-constrained optimal control. *Technical Report 350* 2016.
24. Rozza G, Huynh DP, Patera AT. Reduced basis approximation and a posteriori error estimation for affinely parametrized elliptic coercive partial differential equations. *Archives of Computational Methods in Engineering* 2008; **15**(3):229–275.
25. Chaudhry J, Estep D, Ginting V, Tavener S. A posteriori analysis of an iterative multi-discretization method for reaction–diffusion systems. *Computer Methods in Applied Mechanics and Engineering* 2013; **267**:1–22.
26. Estep D. A posteriori error bounds and global error control for approximation of ordinary differential equations. *SIAM Journal on Numerical Analysis* 1995; **32**(1):1–48.
27. Becker R, Rannacher R. An optimal control approach to a posteriori error estimation in finite element methods. *Acta Numerica 2001* 2001; **10**:1–102.
28. Giles MB, Süli E. Adjoint methods for pdes: a posteriori error analysis and postprocessing by duality. *Acta Numerica* 2002; **11**:145–236.
29. Grepl MA, Maday Y, Nguyen NC, Patera AT. Efficient reduced-basis treatment of nonaffine and nonlinear partial differential equations. *ESAIM: Mathematical Modelling and Numerical Analysis* 2007; **41**(03):575–605.
30. Eftang JL, Patera AT, Rønquist EM. An" hp" certified reduced basis method for parametrized elliptic partial differential equations. *SIAM Journal on Scientific Computing* 2010; **32**(6):3170–3200.
31. Carlberg K. Adaptive h-refinement for reduced-order models. *International Journal for Numerical Methods in Engineering* 2014; .
32. Amsallem D, Farhat C. Interpolation method for adapting reduced-order models and application to aeroelasticity. *AIAA Journal* Jul 2008; **46**(7):1803–1813, doi:10.2514/1.35374. URL `http://dx.doi.org/10.2514/1.35374`.
33. Amsallem D, Zahr MJ, Farhat C. Nonlinear model order reduction based on local reduced-order bases. *Int. J. Numer. Meth. Engng* Jun 2012; **92**(10):891–916, doi:10.1002/nme.4371. URL `http://dx.doi.org/10.1002/nme.4371`.
34. Lohmann R. Model reduction via proper orthogonal decomposition. *Model Order Reduction: Theory, Research Aspects and Applications*. Springer, 2008; 95–109.
35. Lloyd S. Least squares quantization in pcm. *Information Theory, IEEE Transactions on* 1982; **28**(2):129–137.
36. Arthur D, Vassilvitskii S. k-means++: The advantages of careful seeding. *Proceedings of the eighteenth annual ACM-SIAM symposium on Discrete algorithms*, Society for Industrial and Applied Mathematics, 2007; 1027–1035.
37. Mardia KV, Kent JT, Bibby JM. *Multivariate analysis*. Academic press, 1979.
38. Bentley JL. Multidimensional binary search trees used for associative searching. *Commun. ACM* Sep 1975; **18**(9):509–517, doi:10.1145/361002.361007. URL `http://dx.doi.org/10.1145/361002.361007`.